Science Translational Medicine
AAAS

Supplementary Materials for

Human antibody recognizing a quaternary epitope in the Puumala virus glycoprotein provides broad protection against orthohantaviruses

Eva Mittler *et al.*

Corresponding author: Tomas Strandin, tomas.strandin@helsinki.fi; Andrew S. Herbert, andrew.s.herbert4.civ@mail.mil; Mattias N. E. Forsell, mattias.forsell@umu.se; Laura M. Walker, laura.walker@adimab.com; Kartik Chandran, kartik.chandran@einsteinmed.edu

Sci. Transl. Med. **14**, eabl5399 (2022)
DOI: 10.1126/scitranslmed.abl5399

The PDF file includes:

Other Supplementary Material for this manuscript includes the following:

SUPPLEMENTARY MATERIAL

SUPPLEMENTARY MATERIAL AND METHODS

Cell lines

Chinese hamster ovary (FreeStyle™ CHO-S) cells (Gibco, catalog no. R80007ATCC) were cultured in a humidified 37°C, 5% CO_2 incubator in high-glucose Dulbecco's modified Eagle's medium (DMEM, Life Technologies) supplemented with 10% fetal bovine serum (FBS, Atlanta Biologicals), 1% GlutaMAX, and 1% penicillin-streptomycin (both Life Technologies). Human osteosarcoma U2OS cells (ATCC catalog no. HTB-96) were similarly maintained in modified McCoy's 5A medium (Life Technologies) supplemented with the above-named reagents.

Screening Syrian hamsters for human IgG uptake following antibody treatment

ELISA plates were coated with sheep anti-human IgG capture antibody at 0.1 μg per well and blocked with Casein buffer (G Biosciences) at 4°C overnight. Coated plates were washed with PBS/0.1% Tween 20 and blocked with Casein buffer for 1 h at room temperature on a shaker. A standard curve for ADI-42898 was generated by 2-fold dilutions from 500 ng/ml to 15.6 ng/ml of mAb in assay buffer (Casein buffer/10% normal hamster serum). Day 8 serum samples were diluted 1:50 in assay buffer. Standards and diluted samples were added to coated and washed wells and incubated at room temperature for 1 h. Antibodies were detected by adding goat anti-human IgG-HRP conjugate for 1 h. Absorbance values were measured using a SpectraMax 5 (Molecular Devices) and standard curves were generated using GraphPad Prism software and nonlinear regression analysis (sigmoidal, 4PL). Absorbance values from samples with unknown human antibody concentrations were applied to the standard curve to determine the concentration of human IgG. Hamsters that were human IgG negative at day 8 were deemed untreated and removed from the dataset.

Polyreactivity assay

Antibody polyreactivity was measured as described previously (*39*). Briefly, soluble membrane protein and cytosolic protein fractions obtained from CHO cells were biotinylated using NHS-LC-Biotin (Thermo Fisher). Yeast presenting IgGs on their surface were incubated with biotinylated CHO cell preparations on ice. Cells were then washed twice with ice-cold PBSF (PBS containing 0.1% w/v BSA) and incubated with a secondary labelling mix containing ExtrAvidin-R-PE (Sigma-Aldrich catalog no. E4011), anti-human LC-FITC (Southern Biotech catalog no. 2062-02) and propidium iodide for 15 min. The cells were washed twice with PBSF, resuspended and run on a FACSCanto II (BD Biosciences). The mean fluorescence intensity of binding was normalized using control antibodies that display low, medium or high polyreactivity to assess the non-specific binding.

Biolayer interferometry binding analysis with sGn and Gn^H/Gc

For monovalent apparent dissociation constant (K_D) determination, IgG binding to recombinant sGn and Gn^H/Gc antigen was measured by biolayer interferometry (BLI) using a FortéBio Octet HTX instrument (Molecular Devices). For measurements with PUUV Gn^H/Gc, the IgGs were captured (response level 0.5-1.5 nm) to anti-human IgG capture (AHC) biosensors (Molecular Devices) and allowed to stand in PBSF for a minimum of 30 min. After a short (60 s) baseline step in PBSF, the IgG-loaded biosensor tips were exposed (180 s, 1000 rpm of orbital shaking) to the test antigen (100 nM in PBSF) and then dipped (180 s, 1000 rpm of orbital shaking) into PBSF to measure any dissociation of the antigen from the biosensor tip surface. For measurements with sGn, biotinylated antigen (100 nM) was bound to streptavidin capture sensors (Molecular Devices). Binding analysis of IgGs (100 nM) in solution to sGn was performed as described for Gn^H/Gc antigen. Data for which binding responses were 0.1 nm or greater were aligned, inter-step corrected (to the association step) and fit to a 1:1 binding model using the FortéBio Data Analysis Software, version 11.1.

Virus attachment assay

This assay was performed following a previously published protocol (*30*). In short, rVSV-PUUV-Gn/Gc particles bearing mNG-labeled nucleocapsids were incubated with mAb (25 nM) or serum from PUUV-experienced donors at room temperature for 1 h. These rVSV:mAb complexes were spin-occulated onto prechilled U2OS cells at 1,000 rpm and 4°C for 10 min followed by an incubation on a cooling plate at 6°C for 30 min. Unbound virus was removed by washing with cold PBS. Cells were harvested in PBS, fixed with 4% paraformaldehyde on ice and surface-bound virus was detected by flow cytometry by gating on mNG using an LSRII flow cytometer (BD Biosciences) at the Flow Cytometry Core Facility of the Albert Einstein College of Medicine.

Fusion infection assay

rVSV-PUUV-Gn/Gc or -ANDV-Gn/Gc particles were bound to prechilled HUVECs by centrifugation at 2,500 rpm and 4°C for 1 h. Cells were placed on ice and unbound virus washed away with cold PBS. To establish the ideal pH for PUUV Gn/Gc-mediated fusion at the plasma membrane, PBS was replaced with DMEM-F12 media adjusted to pH values ranging from 4.0 to 7.0. Fusion was initiated by incubating HUVECs at 37°C for 1 min, followed by shifting cells back to 4°C. Further rounds of infection were prevented by the exchange of media supplemented with 20 mM NH_4Cl, and infected cells were maintained at 37°C for 12 to 14 h post-infection before automated counting of eGFP+ and mNG+ cells using a Cytation 5 cell imaging multi-mode reader (BioTek Instruments) and a Cell-Insight CX5 imager (Thermo Fisher Scientific) including onboard software. To evaluate the ability of mAbs to inhibit fusion, rVSV-PUUV-Gn/Gc were pre-incubated with increasing amounts of mAb (0.005 to 5.0 nM) for 1 h at 4°C prior to centrifugation onto HUVECs. Fusion was initiated with an optimal pH of 5.5 and viral infectivity was scored as described above.

SUPPLEMENTARY FIGURES & TABLES

Fig S1

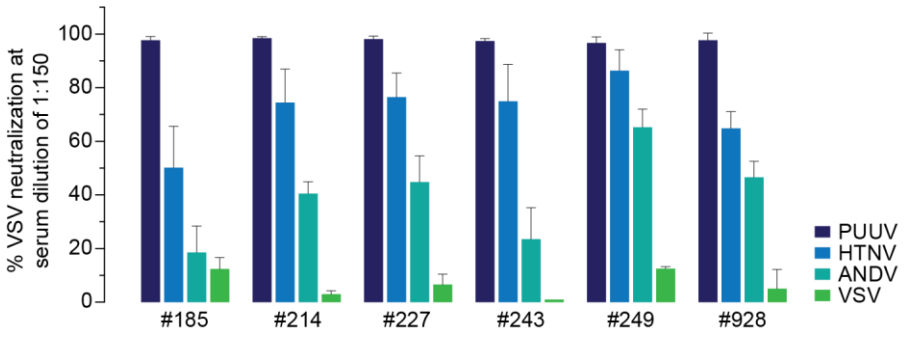

Fig. S1: Neutralization activity of PUUV convalescent patient sera.

Neutralization of rVSV-PUUV, -HTNV, and -ANDV-Gn/Gc or -VSV-G infection in the presence of sera from six PUUV-experienced donors (1:150 dilution). Averages ± SD, n>4 from two to three experiments (PUUV and HTNV); n=4 from two experiments (ANDV); n=2 from one experiment (VSV).

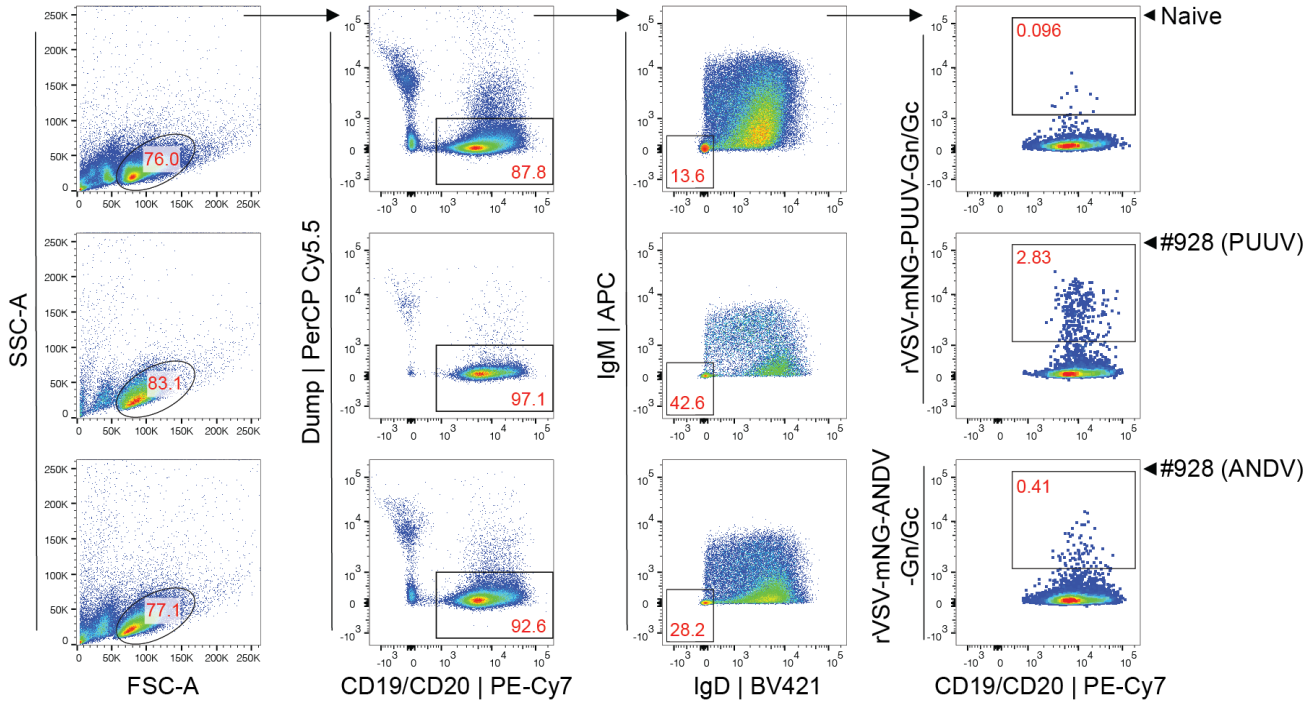

Fig. S2: Flow gating strategy for isolation of Gn/Gc-reactive memory B cells.

Representative gating strategy to sort single B cells specific for hantaviral Gn/Gc. SSC-A: Side scattered light; FSC-A: Forward scattered light.

Fig S3

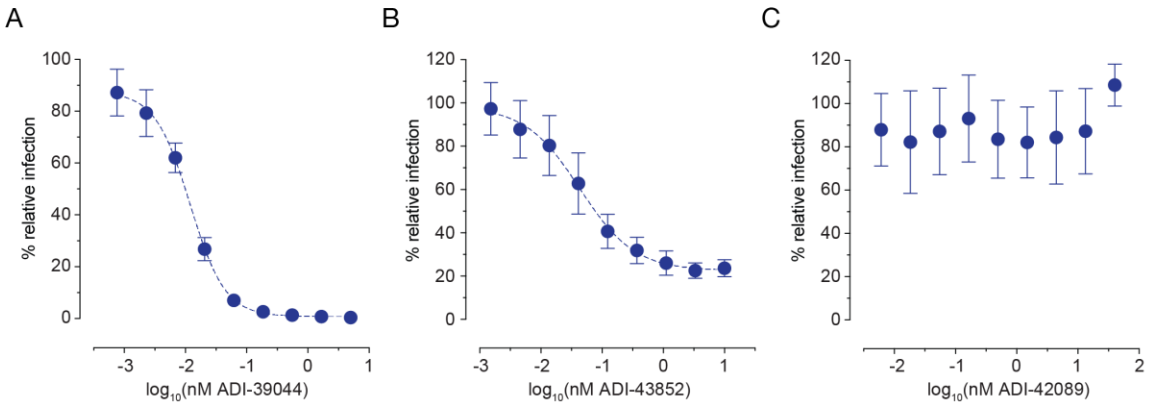

Fig. S3: Curves for selected mAbs with different neutralization patterns.

Neutralization of rVSV-HTNV-Gn/Gc by (**A**) ADI-39044, a neutralizing mAb; (**B**) ADI-43852, a mAb leaving a non-neutralized virus fraction; (**C**) ADI-42089, a mAb lacking neutralization activity. Averages ± SD, *n*=6 for two experiments.

Fig S4

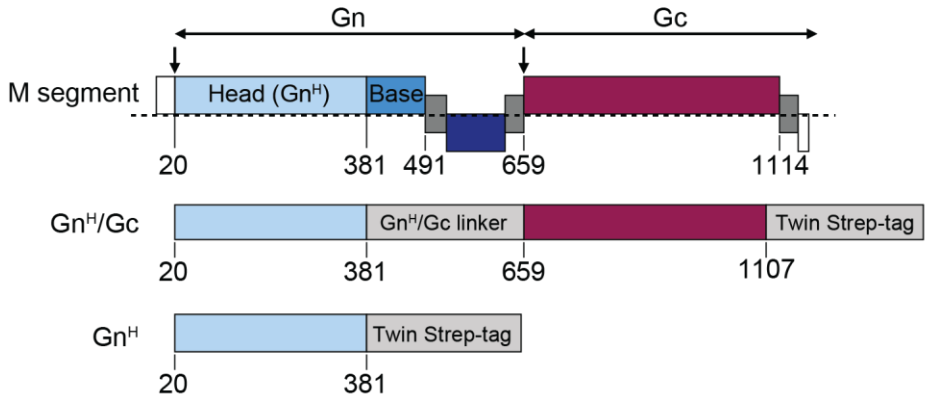

Fig. S4: Domain organization of PUUV Gn/Gc, Gn^H/Gc and Gn^H.

(*Top*) Diagram of PUUV GPC encoded by a single open reading frame of the genomic RNA segment M. Cleavage sites are marked by arrows. Dashed line indicates the viral membrane. (*Middle*) Schematic of the single-chain Gn^H/Gc construct spanning the Gn head domain, Gn^H (aa 20-381) and Gc (aa 659-1107), and bypassing the trans-membrane segments in the precursor polyprotein by a soluble, 43-aa long, flexible linker. A Twin Strep-tag needed for protein purification was encoded in frame at the C-terminal end of the Gc sequence. (*Bottom*) Diagram of the single Gn^H domain (aa 20-381), also containing a Twin Strep-tag connected to its C-terminus.

Fig S5

A

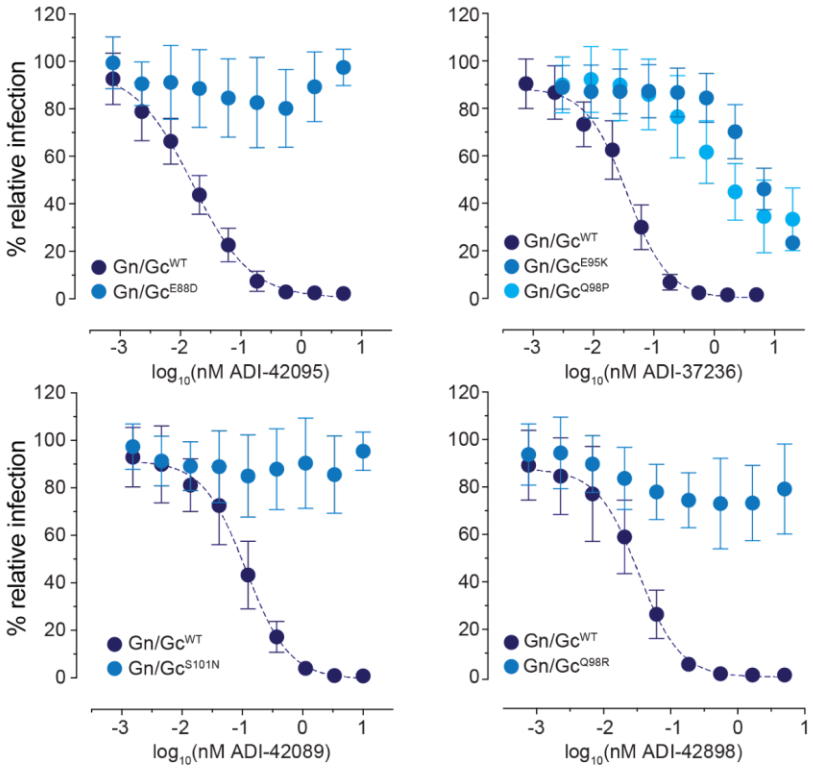
% relative infection
Gn/Gc^WT
Gn/Gc^E88D
log10(nM ADI-42095)
Gn/Gc^WT
Gn/Gc^E95K
Gn/Gc^Q98P
log10(nM ADI-37236)
Gn/Gc^WT
Gn/Gc^S101N
log10(nM ADI-42089)
Gn/Gc^WT
Gn/Gc^Q98R
log10(nM ADI-42898)

B

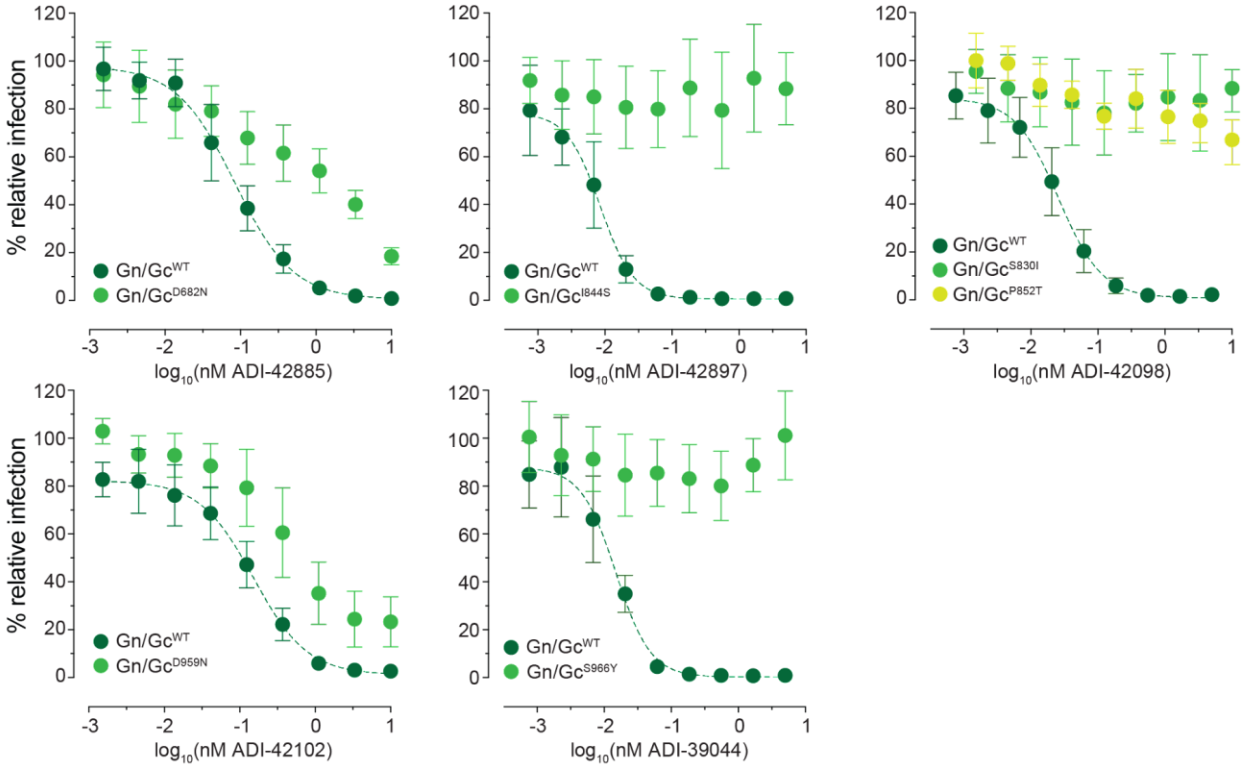
% relative infection
Gn/Gc^WT
Gn/Gc^D682N
log10(nM ADI-42885)
Gn/Gc^WT
Gn/Gc^I844S
log10(nM ADI-42897)
Gn/Gc^WT
Gn/Gc^S830I
Gn/Gc^P852T
log10(nM ADI-42098)
Gn/Gc^WT
Gn/Gc^D959N
log10(nM ADI-42102)
Gn/Gc^WT
Gn/Gc^S966Y
log10(nM ADI-39044)

Fig. S5: Characterization of rVSV-PUUV-Gn/Gc neutralization-escape mutants.

Capacity of mAbs to neutralize rVSV-PUUV-Gn/Gc bearing neutralization-escape variants in its Gn (**A**) or Gc (**B**) subunit. Averages ± SD, *n*=6-12 from two to four experiments.

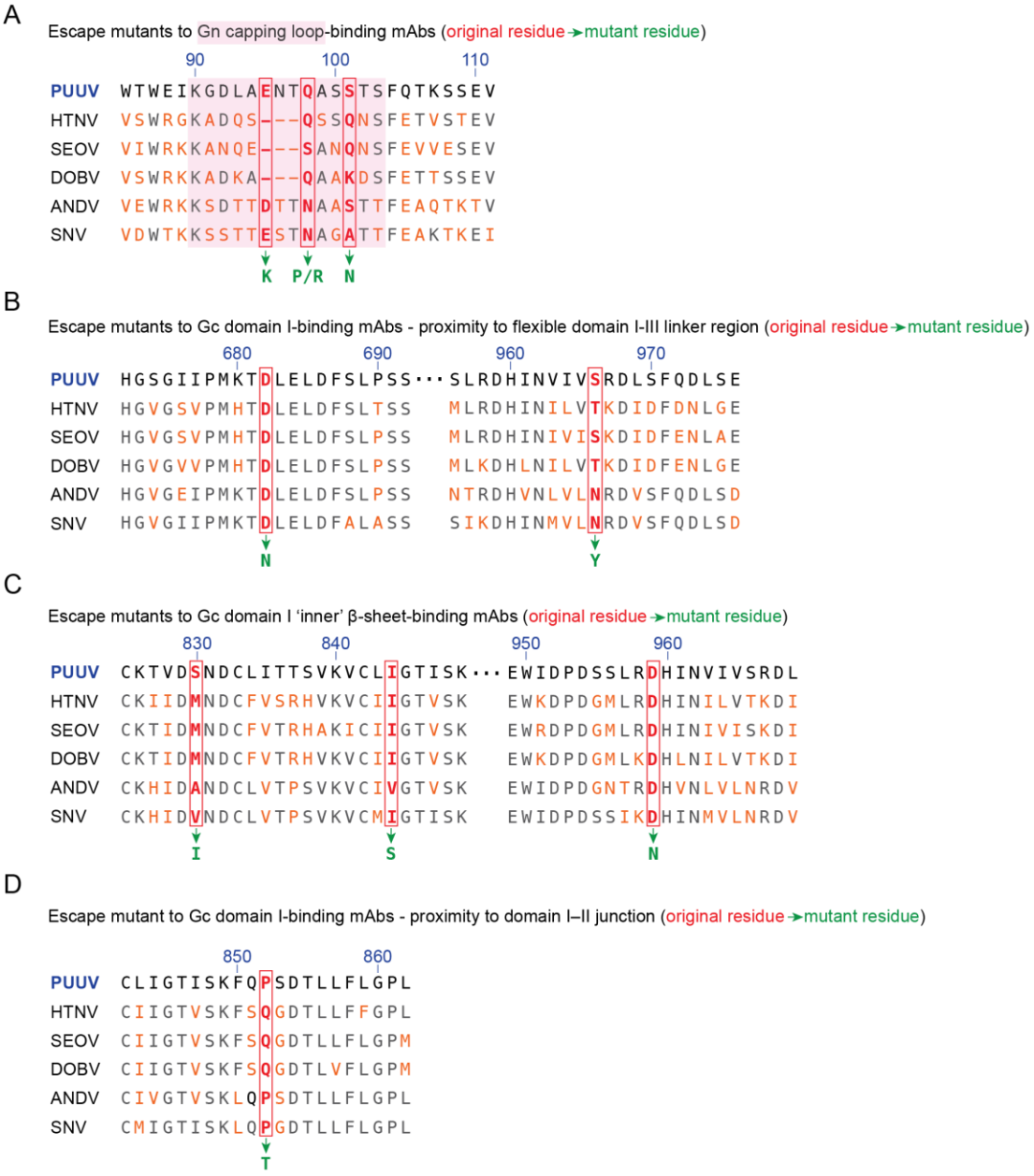

Fig. S6: Locations of viral neutralization escape mutations in PUUV Gn/Gc.

Aa sequence alignment of regions of OWH and NWH Gn/Gc encompassing escape mutations are shown (PUUV Gn/Gc numbering). Escape mutations are found in the Gn (**A**) and Gc (**B-D**) subunit. Gray, conserved residues. Orange, divergent residues. Positions of escape mutations are boxed and labeled in red, and the residue changes are indicated in green. In (A) the location of the Gn capping loop is shaded in pink.

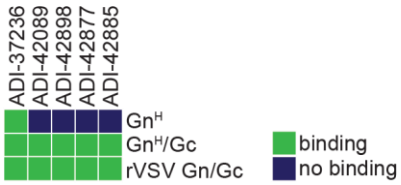

Fig. S7: Binding activity of mAbs to PUUV Gn/Gc subdomain constructs.

Heatmap presents binding activity of mAbs to PUUV Gn^H, Gn^H/Gc and rVSV-PUUV-Gn/Gc (also see Fig. S4). Binding of mAbs to rVSV-PUUV-Gn/Gc was determined in a single concentration mAb spot ELISA; mAbs crossing an ELISA signal threshold of 0.3 were defined as binders. Binding of mAbs to PUUV Gn^H and Gn^H/Gc was determined by BLI; mAbs presenting with binding responses >0.1 nm were defined as binders.

Fig S8

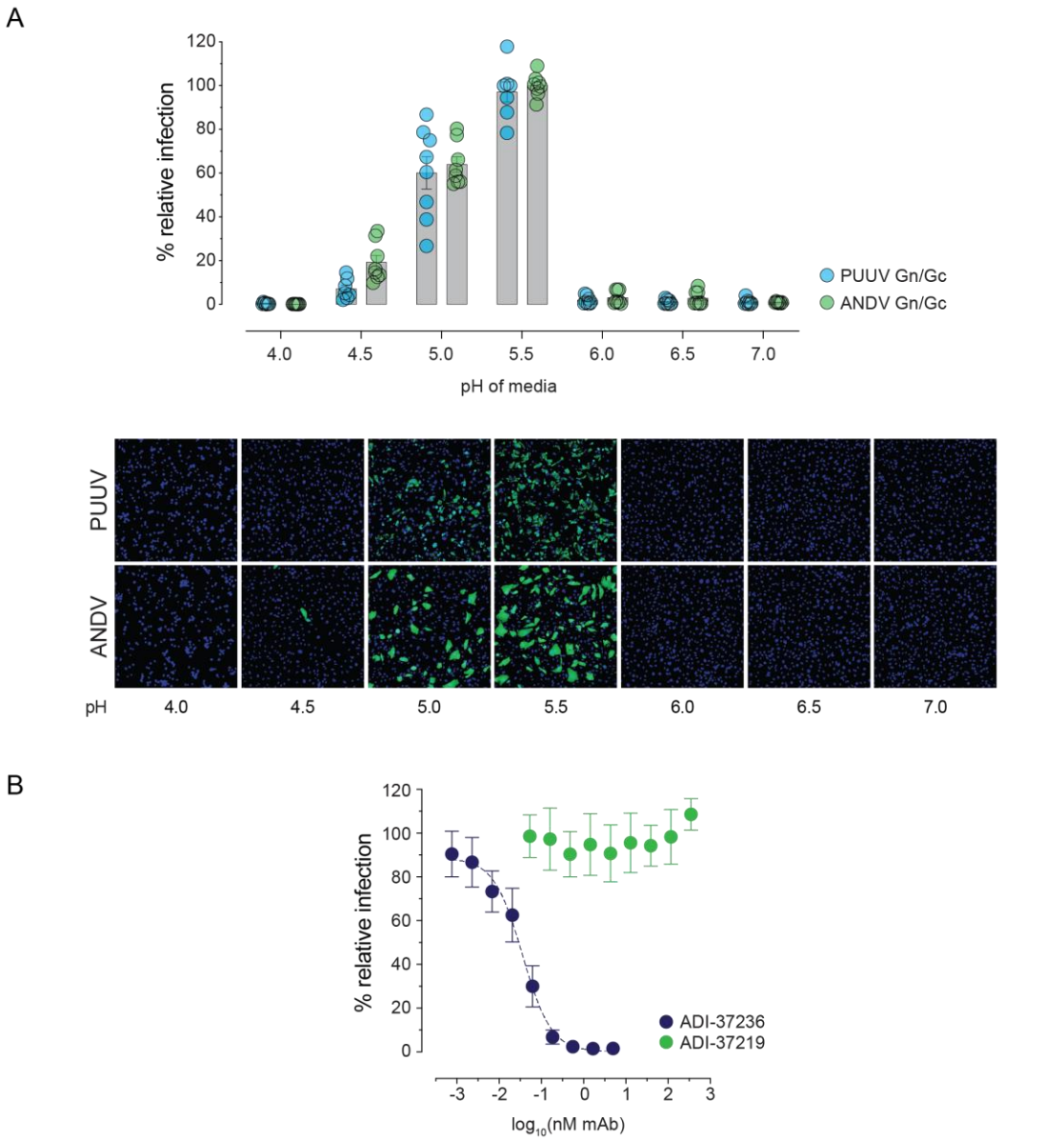

Fig. S8: Establishment of fusion-infection assay with rVSV-PUUV-Gn/Gc.

(**A**) Identification of optimal pH for PUUV Gn/Gc-induced fusion-infection. rVSV particles were bound to pre-chilled HUVECs, incubated with media adjusted to pH 7.0 - 4.0, followed by fusion-infection. rVSV-ANDV-Gn/Gc particles served as positive control. (*Top*) Averages ± SD, $n>7$ from three experiments. (*Bottom*) Representative images of infected eGFP+ or mNG+ cells (pseudo-colored green) detected by fluorescence microscopy. (**B**) Capacity of ADI-37219 and ADI-37236 to neutralize rVSV-PUUV-Gn/Gc. Averages ± SD, $n=6$ from two experiments (ADI-37219) and $n=9$ from three experiments (ADI-37236).

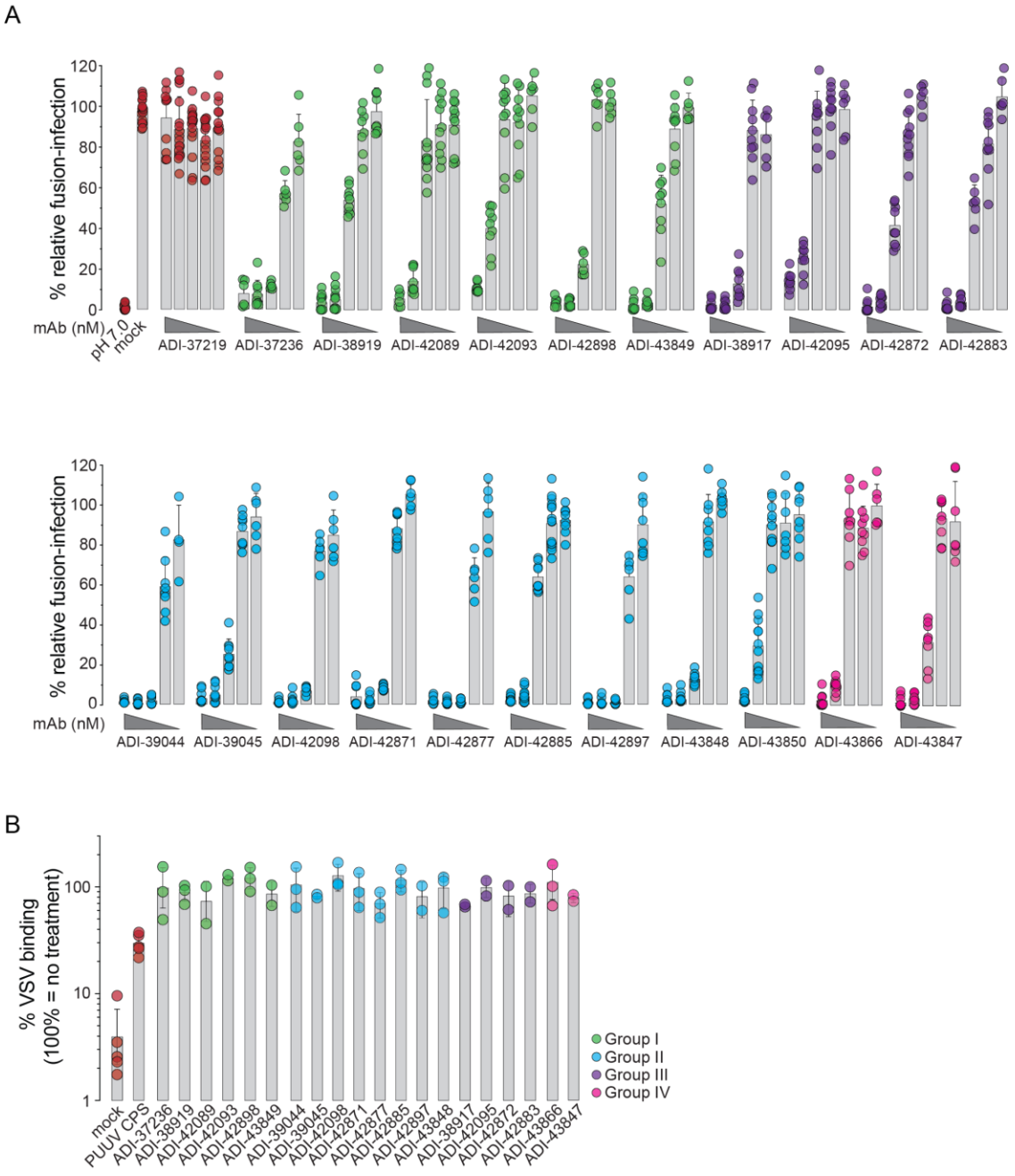

Fig. S9: Mechanistic basis of mAb-dependent inhibition of virus infection.

(**A**) Capacity of mAbs to block PUUV Gn/Gc-mediated fusion-infection. rVSV-PUUV-Gn/Gc particles were pre-incubated with decreasing amounts of indicated mAbs (50 nM to 0.005 nM), followed by fusion-infection of HUVECs. ADI-37219, a non-neutralizing mAb, was included as a negative control (also see

Fig. S8B). Data points are colored according to the mAb's competition group assignments defined in Fig. 3. Averages ± SD, *n*=6-18 from two to six experiments. (**B**) Capacity of mAbs to block attachment of virus particles to host cells. Pre-titrated amounts of rVSV-mNG-P-PUUV-Gn/Gc were incubated with mAbs at 25 nM (or PUUV convalescent patient serum (CPS) at a 1:100 dilution). Binding of rVSV:mAb complexes to U2OS cells was determined by flow cytometry. Data points are colored according to the mAb's competition group assignments defined in Fig. 3. Averages ± SD, *n* = two to three experiments.

Fig S10

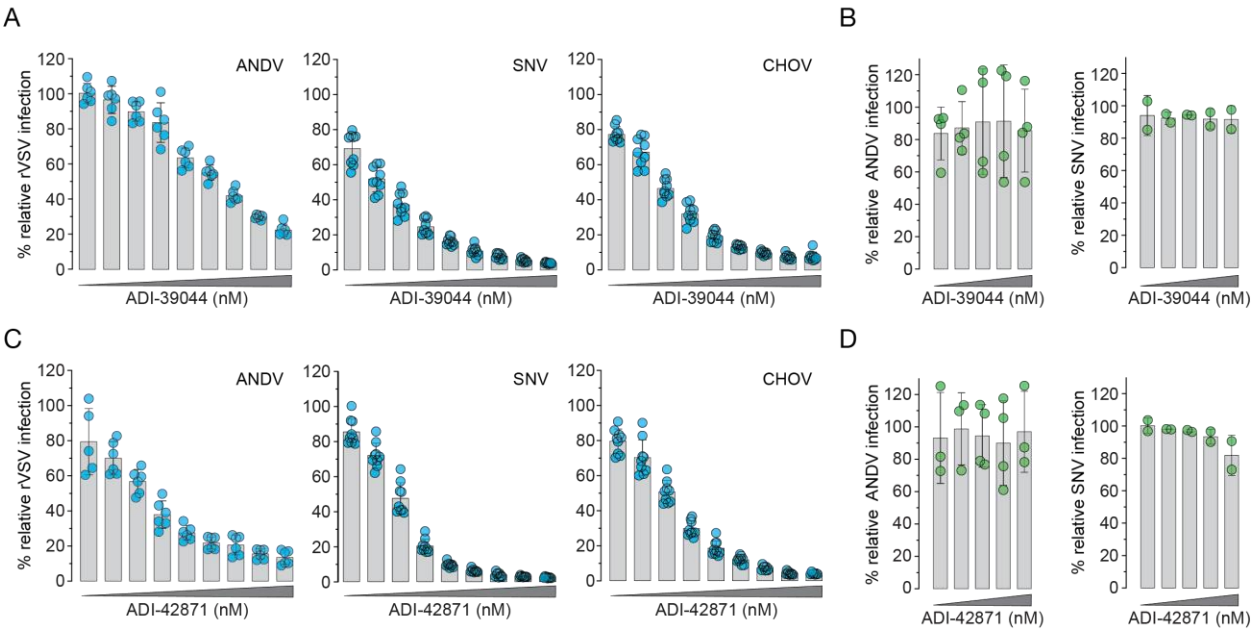

Fig. S10: Activity of Group II mAbs against NWH Gn/Gc-mediated infection.

(**A** and **C**) Capacity of Group II nAbs, ADI-39044 and ADI-42871 to block infection by rVSV-ANDV, -SNV and -CHOV-Gn/Gc on Vero cells. mAb dilution series started at 100 nM (ADI-39044, all three rVSVs), 40 nM (ADI-42871, rVSV-ANDV-Gn/Gc) or 10nM (ADI-42871, rVSV-SNV- and CHOV-Gn/Gc) followed by 3-fold dilutions. Averages ± SD, *n*=6 from two experiments. (**B** and **D**) Capacity of Group II nAbs, ADI-39044 and ADI-42871 to inhibit infection by authentic NWH, ANDV and SNV on HUVECs. mAb dilution series started at 100 nM followed by 5-fold dilutions. Averages ± SD, *n*=2 from one experiment (SNV), and *n*=4 from two experiments (ANDV).

Fig S11

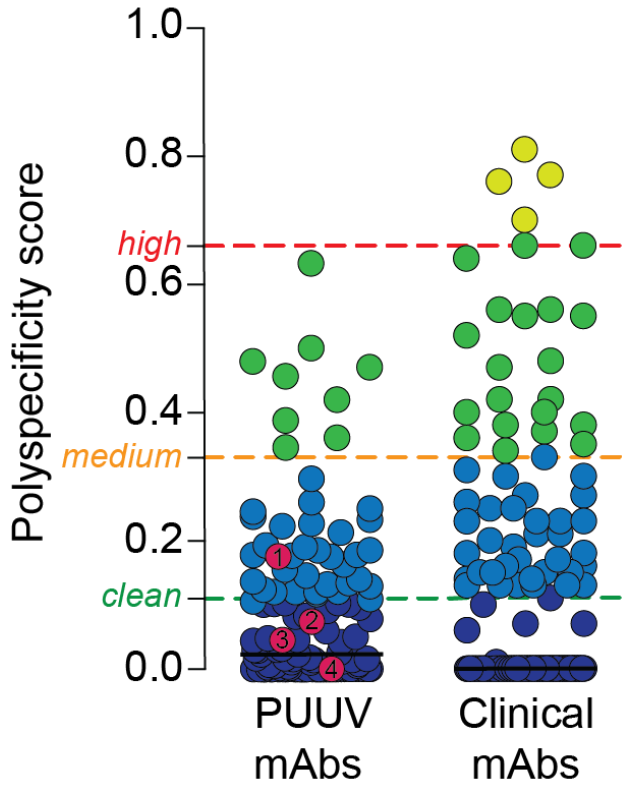

Fig. S11: Polyreactivity of mAbs isolated from PUUV-experienced donors.

Polyreactivity was determined using a previously described assay (*39*). Thresholds for high, medium, and low polyreactivity are indicated by dashed lines. Polyspecificity scores for 137 clinical stage mAbs are shown for comparison. Bar indicates median. mAbs tested in bank vole PUUV challenges are marked: 1 = ADI-42898; 2 = ADI-42877; 3 = ADI-38919; 4 = ADI-42098.

Table S1

A

Tree Label	Virus Name	Strain/Isolate	GenBank #
ANDV	Andes virus	Chile-9717869	MT956623.1
BAYV	Bayou virus	HV F0260003	GQ244521.1
BCCV	Black creek canal virus		L39950.1
CHOV	Choclo virus	588	KT983772.1
DOBV	Dobrava-Belgrade virus	Ano-Poroia/Af19	NP_942554.1
HTNV	Hantaan virus	76-118	Y00386.1
LGNV	Laguna Negra virus	510B	AF005728.1
MPRLV	Maporal virus	HV-97021050	NC_034552.1
PHV	Prospect Hill virus	M3	X55129.1
PUUV	Puumala virus	CG1820/POR	ALI59825.1
SEOV	Seoul virus	SR-11	M34882.1
SNV	Sin Nombre virus	NM H10	KT885045.1
TULV	Tula virus	Moravia/5302v/95	NC_005228.1

B

	ANDV	SNV	CHOV	MPRLV	LGNV	BAYV	BCCV	PUUV	HTNV	SEOV	DOBV	TULV
ANDV		78	83	85	86	76	75	66	55	54	54	68
SNV	78		78	77	77	80	80	67	55	53	54	69
CHOV	83	78		83	82	77	76	65	54	53	55	66
MPRLV	85	77	83		81	75	74	65	55	53	54	67
LGNV	86	77	82	81		75	76	65	55	54	54	67
BAYV	76	80	77	75	75		89	65	55	54	54	68
BCCV	75	80	76	74	76	89		66	55	53	53	68
PUUV	66	67	65	65	65	65	66		53	54	53	79
HTNV	55	55	54	55	55	55	55	53		77	77	55
SEOV	54	53	53	53	54	54	53	54	77		77	54
DOBV	54	54	55	54	54	54	53	53	77	77		55
TULV	68	69	66	67	67	68	68	79	55	54	55	

Table S1: GPC amino acid sequence analyses related to Fig. 1A.

(**A**) GPC amino acid sequences used for the construction of Fig. 1A. (**B**) Pairwise aa sequence comparison of orthohantavirus GPCs shown in (A) as given in % identity.

A

	PUUV patients (n=45) mean (range)	Reference interval
Age (years)	48 (18-75)	
Sex (male/female)	25/20 (56%/44%)	
C-reactive protein, max (mg/L)	85 (16-214)	<3
Leukocyte count, max (10e9/L)	10.7 (6.7-22.2)	3.5-8.8
Platelet count, min (10e9/L)	82 (11-310)	145-387
S-creatinine, max (µmol/L)	404 (66-1548)	<90/<105*
S-lactate dehydrogenase, max (µkat/L)	6 (1.1-11.8)	<3.4
PT INR, max	1.1 (0.9-2.3)	<1.2
APTT, max (secs)	31 (23.9-39.1)	24.0-36.0
P-albumin, min (g/L)	31 (20-44)	36-45

B

	B Cell Donor					
	1	2	3	4	5	6
Sample #	185	214	227	243	249	928
Age (years)	65	49	69	39	38	70
Sex (male/female)	F	M	F	M	F	F
Day after disease onset	67	70	63	63	37	90
Laboratory findings						
C-reactive protein, max (mg/L)	42	48	68	138	58	56
Leukocyte count, max (10e9/L)	10.1	9.5	11.5	14.3	15.2	7.8
Platelet count, min (10e9/L)	133	87	146	18	11	151
S-creatinine, max (µmol/L)	94	886	192	769	178	403
S-lactate dehydrogenase, max (µkat/L)	4.2	6.3	4.6	8.7	5.4	4.9
PT INR, max	1.1	1.0	1.0	1.1	1.2	1.0
APTT, max (secs)	28.3	28.7	26.6	38.5	31.2	27.5
P-albumin, min (g/L)	N.D.	41	37	43	38	28

Table S2: Demographic and laboratory characteristics of PUUV cohort donors during acute phase of disease.

(**A**) PUUV patients displayed typical symptoms for HFRS such as acute onset of fever, myalgia, head and abdominal pain. Signs of thrombocytopenia and transient renal failure were frequent. The maximum or minimum values during the acute phase of the disease are presented. *, reference values for females and males, respectively. (**B**) Table of metadata from six PUUV convalescent patients prioritized for isolation

of memory B cells reactive to hantaviral Gn/Gc. APTT, Activated Partial Thromboplastin Time; PT INR, Prothrombin Time - International Normalized Ratio. ND, not determined.